Photoionization indicators of optical mixing of different-parity degenerate Rydberg states

R. Parzyński, M. Sobczak, and A. Wójcik
Faculty of Physics, Adam Mickiewicz University, Umultowska 85, 61-614 Poznań, Poland
(Received 16 April 1999; revised manuscript received 29 June 1999; published 13 January 2000)

We discuss a photoionization version of the photoexcitation model of Corless and Stroud [Phys. Rev. Lett. **79**, 637 (1997)]. In the photoexcitation model, a *np* hydrogenic state of $n \gg 1$ was excited from the ground $1s$ state and the excited population was allowed to migrate to other angular momentum states within the one *n* only due to strongly nonresonant electric-dipole $|\Delta n|=0$, $|\Delta l|=1$ Rydberg-to-Rydberg couplings. When, as is the essence of the photoexcitation model, the same one *n*-manifold approximation is made in the model of high-*n* Rydberg-state photoionization, a number of interesting photoionization effects are obtained. Among them, the most spectacular seems to be the emission of photoelectrons in the ''forbidden'' directions and the suppression of ionization when compared to the Fermi golden rule predictions. However, we show on the basis of an approximate analysis that these photoionization effects can be strongly diminished when additional *n* manifolds around the selected one are included in the model. Thus, we conclude that the one *n*-manifold approximation overestimates results when applied to the problem of high-*n* Rydberg-state photoionization.

PACS number(s): 32.80.Rm, 42.50.Hz

I. INTRODUCTION

The Rydberg atom, real or a model, is a favorite system for the study of a variety of quantum transitions caused by an intense laser-photon flux. For example, Corless and Stroud [1] have recently considered a model of excitation of an *np* hydrogenic state of $n \gg 1$ from the ground $1s$ state, differing substantially from other models. In this model the population from the directly excited *np* state migrated to higher-angular-momentum states, all sharing the same principal quantum number *n*, due to a sequence of $|\Delta l|=1$ electric-dipole transitions. Each coupling between any pair of the degenerate states differing in *l* by 1 was thus strongly nonresonant with the detuning equal to the frequency of the electromagnetic field. For such a coupling to be non-negligible the detuning must have been compensated by the Rabi frequency for the Rydberg-to-Rydberg coupling. If the electromagnetic field is linearly polarized along the *z* axis, this Rabi frequency for the coupling from the $n,l-1,m=0$ to $n,l,m=0$ states is [2] $\Omega^{n,l,0}_{n,l-1,0}=(e\varepsilon_0/\hbar)z^{n,l,0}_{n,l-1,0}=3.3\times 10^8\, nl(n^2-l^2)^{1/2}(4l^2-1)^{-1/2}I^{1/2}$, where *I* is the electromagnetic-field intensity expressed in W/cm^2. Thus, for $l \ll n$ and, e.g., $n=30$, an enormous dipole moment for the coupling results in the Rabi frequency approaching an optical frequency already at a relatively low critical intensity of the order of 10^{10} W/cm^2. The appropriate calculations performed by Corless and Stroud [1] gave evidence for indirect excitation from the $1s$ state of a broad range of different-parity angular momentum states, all of the same *n*. Obviously, the nonresonant $|\Delta l|=1$ Rydberg-to-Rydberg couplings in question differ deeply in their nature from the $|\Delta l|=2$ Raman couplings considered earlier by other authors [3–10] in the familiar rotating-wave approximation. One spectacular difference is that the latter ones mix a given parity subset of Rydberg states only.

The aim of the present paper is to study a photoionization version of the original excitation model of Corless and Stroud. Instead of the ground state, we let the initial population be in a high Rydberg state *nl* (of $n=30$, for example) and add the ionization continuum to which the Rydberg states are damped (Fig. 1). In fact, we are interested in the effect of the nonresonant $|\Delta l|=1$ migration of the population from the initial *l* state towards other bound *l* states on the photoionization characteristics, namely, the photoelectron angular distributions and the total ionization yield. When solving analytically this photoionization model we neglect, as in the original excitation model, all other *n* manifolds except one. In the case of photoionization, the selected *n* manifold is determined by the initial preparation of the atom. At first sight, this neglect seems to be justified when one compares quasiclassical dipole moments for the $\Delta n=0$ and $\Delta n \neq 0$ transitions. As shown [1], the dipole moments tend to diminish for increasing Δn and, e.g., for $\Delta n=1$ the dipole moment is smaller than that for $\Delta n=0$ by as much as a factor of 5, provided that $l \ll n$. However, we will show, along an approximate analysis, that the interesting photoionization effects, predicted by the exactly solvable model with only one *n* manifold, can be drastically diminished by the presence of the neighboring *n* manifolds. This raises the question of validity of the one *n*-manifold approximation which can be resolved, e.g., by experimental verification of some results of the present paper.

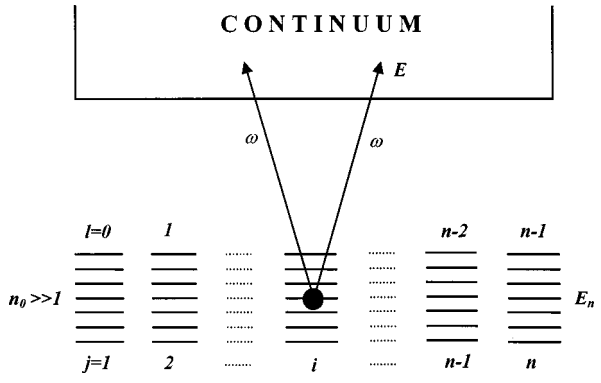

FIG. 1. The model of photoionization from an $n_0 l_i$ Rydberg state ($n_0 \gg 1$), including the $|\Delta l|=1$ Rydberg-to-Rydberg couplings between *l* series. This model is a modification of the model of photoexcitation of Corless and Stroud [1]. Here, *j* numbers different *l* series ($l_j=j-1$).

Section II is devoted to solving the photoionization model with one n manifold only. It gives basic equations for the population dynamics of the relevant states and their solutions in the perturbative approximation for the bound-free transitions. Then, the general solution is applied to a special case when the photoionization starts from an *ns* Rydberg state and two photoionization indicators of the $|\Delta l|=1,\Delta n=0$ Rydberg-to-Rydberg couplings are defined. Moreover, the results of detailed calculations for $n=30$ are presented and discussed. In Sec. III, we include the neighboring n manifolds assuming pulses shorter than the Kepler period of the initially populated Rydberg state. The generalization made allows us to formulate the final conclusion of the negative effect of these additional n manifolds on the results obtained within the one n-manifold approximation.

II. MODEL OF PHOTOIONIZATION WITH ONE n MANIFOLD

A. The solution

In each l series of Fig. 1, we leave only one state ($n_0=n$). The chain of l states attributed to a given $n\gg 1$ (energy E_n), with only one l state initially occupied (i), is coupled to the atomic continuum (energy E) by an optical pulse of frequency ω, linearly polarized in the z direction. We apply the long-wavelength approximation, i.e., choose the electric field as uniform within the atom, $\varepsilon(t)=f(t)\,\varepsilon_0\cos\omega t$, where ε_0 is the amplitude and $f(t)$ the pulse envelope. In our formulation, the pulse interacts with our model atom through the dipole Hamiltonian $V(t)=-ez\varepsilon(t)=-Vf(t)\cos\omega t$ with $V=ez\varepsilon_0$. The wave function Ψ of the system is then governed by the total Hamiltonian $H=H_0+V(t)$, where H_0 is the unperturbed Hamiltonian whose eigenfunctions and eigenvalues are ϕ_j and $\hbar\omega_j$, respectively. By the common expansion $\Psi=\Sigma_j C_j\phi_j\exp(-i\omega_j t)$, one obtains from the Schrödinger equation $(i\hbar)\,d\Psi/dt=H\Psi$ a set of textbook equations [11] for the expansion amplitudes C_j. Any two expansion amplitudes in this set are interrelated by the matrix element $V_{jk}=\langle\phi_j/e\varepsilon_0 z/\phi_k\rangle$ being nonzero for the $|\Delta l|=1$ couplings within the same n manifold. This allows the $|\Delta l|=1$ transitions along the chain of degenerate discrete l states of our model because nonzero expansion amplitudes C_j imply nonzero probability (transition) amplitudes $S_j=\langle\phi_j/\Psi\rangle=C_j\exp(-i\omega_j t)$.

However, an apparent paradox would have appeared if we had simply replaced the dipole interaction Hamiltonian $V(t)=-ez\varepsilon(t)$ by the minimal-coupling interaction Hamiltonian $V'(t)=-(e/m)p_z A(t)$ in the above matrix elements. Because the momentum operator p_z has vanishing matrix elements between degenerate states $[(p_z)_{jk}\sim\omega_{jk}z_{jk}]$, such a replacement would result, at first look, in no transitions along the chain of discrete l states of our model. This conclusion is incorrect and originates in overlooking the need of transformation of wave functions when coming to the interaction Hamiltonian in the minimal-coupling form $V'(t)$. Clarifying discussions of this point can be found in Refs. [11–15], for example. Briefly, the dipole interaction Hamiltonian $V(t)$ and the minimal-coupling interaction Hamiltonian $V'(t)$ appear in two forms of the Schrödinger equation which are related by the unitary gauge transformation $T=\exp[iezA(t)/\hbar]$. By this transformation, the Schrödinger equation considered by us, $(i\hbar)\,d\Psi/dt=H\Psi=[H_0+V(t)]\Psi$ is converted into $(i\hbar)d\Psi'/dt=H'\Psi'=[H_0+V'(t)]\Psi'$, where $\Psi'=T\Psi$. So, choosing the interaction Hamiltonian in the minimal-coupling form $V'(t)$ we have to work with wave functions transformed by the operator T, i.e., $\Psi'=T\Psi$ and $\phi'=T\phi$. With the use of the transformed (primed) Schrödinger equation, the transition amplitude is $S'_j=\langle\phi'_j/\Psi'\rangle=\langle\phi_j/T^\dagger/\Psi'\rangle=\Sigma_k T^\dagger_{jk}C'_k\exp(-i\omega_k t)$, where $T^\dagger_{jk}=\langle\phi_j/T^\dagger/\phi_k\rangle$, and the expansion amplitudes $C'_k[\Psi'=\Sigma_l C'_l\,\phi_l\exp(-i\omega_l t)]$ fulfill the same equations as C_k but with the change $V(t)\to V'(t)$. Let us see that with overlooking the wave-function transformation, $T^\dagger_{jk}$ would be replaced by the Kronecker symbol δ_{jk}, resulting in an incorrect relation between the transition amplitudes S'_j and the expansion amplitudes C'_j and the paradox stated. Rigorously, for the model with one n manifold and the continuum neglected in it for simplicity, $C'_k=C'_k(t)=C'_k(t_0)$ with t_0 standing for the turn-on time of the atom-field interaction. In the inverted form, the relation between the nonequivalent amplitudes S'_j and C'_k reads $C'_k=\exp(i\omega_k t)\Sigma_l T_{kl}S'_l$. After using the initial condition, $S'_l=\delta_{li}$ at $t=t_0$, the last equation converts into $C'_k(t_0)=\exp(i\omega_k t_0)T_{ki}(t_0)$. As a result, the transition amplitude is $S'_j=\Sigma_k T^\dagger_{jk}T_{ki}(t_0)\exp[-i\omega_k(t-t_0)]=\exp[-i\omega_j(t-t_0)][T^\dagger T(t_0)]_{ji}$, where we made use of the fact that $\omega_k=\omega_j$ in the case of degeneracy. For example, to lowest order in electromagnetic field, $T=1+iezA(t)/\hbar$, and then one obtains $S'_j=\exp[-i\omega_j(t-t_0)](ie/\hbar)z_{ji}\int\varepsilon(t')dt'$. Obviously, the obtained $S'_j=\langle\phi'_j/\Psi'\rangle$ is nonzero and, as required by gauge-invariant physical quantities [11–15], identical with $S_j=\langle\phi_j/\Psi\rangle$, if the latter transition amplitude is calculated in the first-order perturbation theory. This removes the apparent paradox.

As our emphasis is on the properties of the electron in the continuum, we start with writing down the equation for $C_E(t)$, i.e., the transition amplitude (with accuracy to phase) to such a state. With no rotating-wave approximation made, this equation reads

$$\frac{dC_E(t)}{dt}=\frac{i}{\hbar}f(t)\cos(\omega t)e^{i(E-E_n)t/\hbar}\sum_{j=1}^{n}V_{Ej}C_j(t), \quad (1)$$

where $V_{Ej}=\langle E|e\varepsilon_0 z|j\rangle$ is the time independent part of the bound-free matrix element for the atom-field interaction Hamiltonian. On the other hand, the population amplitudes $C_j(t)$ of Rydberg states fulfill the integrodifferential equation

$$\frac{dC_j(t)}{dt}=\frac{i}{\hbar}f(t)\cos(\omega t)\left[\sum_{j'=1}^{n}V_{jj'}C_{j'}(t)+\int_0^\infty dE V_{jE}C_E(t)e^{-i(E-E_n)t/\hbar}\right], \quad (2)$$

with $V_{jj'}=\langle j/e\varepsilon_0 z/j'\rangle$ being the bound-bound analog of

V_{Ej}. Under the familiar assumption of weak E dependence of V_{Ej}, we perform the energy integration in Eq. (2), using the formally time-integrated Eq. (1). After this procedure, Eq. (2) becomes

$$\frac{dC_j(t)}{dt} = if(t)\cos(\omega t)\sum_{j'=1}^{n}\Omega_{jj'}C_{j'}(t) - \frac{\pi}{\hbar}[f(t)\cos(\omega t)]^2\sum_{j'=1}^{n}V_{jE}V_{Ej'}C_{j'}(t), \quad (3)$$

where $\Omega_{jj'}=V_{jj'}/\hbar$ is the Rydberg-to-Rydberg Rabi frequency for states differing by 1 in l, and the second term describes either the ionization damping of a given Rydberg state ($j'=j$) or the $|\Delta l|=2$ nonresonant Raman transitions between Rydberg states via the atomic continuum. The latter ones received much attention in the past [3–10] in the rotating-wave approximation and, thus, are not of interest to us now. Throughout this paper we deal with such laser frequencies ($\omega=0.2$ a.u.) and intensities for which $\Omega_{jj'}$ is the leading coupling parameter. We, thus, simply drop the second term in Eq. (3). Then, the calculation of $C_E(t)$ from Eq. (1) corresponds to the purely perturbative treatment of the bound-free transitions.

We introduce $A_{jj'}=\Omega_{jj'}/\Omega_{12}$, i.e., scale all Rydberg-to-Rydberg Rabi frequencies in terms of the Rabi frequency $\Omega_{12}=\Omega$, i.e., that for the first coupling in the chain. Equation (3), with the second term dropped, is then of the matrix-form equation

$$\frac{dC}{dt}=a(t)AC, \quad (4)$$

where $a(t)=i\Omega f(t)\cos\omega t$, C is the one column matrix of the population amplitudes $C_j(t)$, and A is the matrix of the scaled Rabi frequencies. The latter matrix has only two nonzero diagonals, the one above and the other below the main diagonal. We prefer to solve Eq. (4) by the standard diagonalization procedure [16] of A. If P is a matrix that diagonalizes A, i.e., such that $P^{-1}AP=A_D$, then we introduce a new matrix $G=P^{-1}C$ satisfying the matrix equation $dG/dt=a(t)A_DG$. The solution of the latter equation is $G(t)=\Lambda(t)G(t_0)=\Lambda(t)P^{-1}C(t_0)$, where t_0 defines the turn-on time of the optical pulse, and $\Lambda(t)$ is a diagonal matrix whose elements are $\Lambda_{j'j}=\exp[\lambda_j S(t)]\delta_{j'j}$, with λ_j being a given eigenvalue of A and $S(t)=\int_{t_0}^{t}dt'a(t')=i\Omega\int_{t_0}^{t}dt'f(t')\cos\omega t'$. The diagonalizing matrix P, whose jth column includes the eigenvector of A corresponding to the λ_j eigenvalue, is orthogonal ($P^{-1}=P^T$). This, along with the back-transformation from G to C, results in the following solution to Eq. (4):

$$C(t)=P\Lambda(t)P^TC(t_0) \quad (5)$$

or

$$C_j(t)=\sum_{k,m=1}^{n}P_{jk}P_{mk}C_m(t_0)e^{\lambda_k S(t)}. \quad (6)$$

In the special case where only one state is initially populated [$C_m(t_0)=\delta_{mi}\exp(i\omega_m t_0)$], the last equation reduces to

$$C_j(t)=e^{i\omega_i t_0}\sum_{k=1}^{n}P_{jk}P_{ik}e^{\lambda_k S(t)}. \quad (7)$$

We shall use Eq. (7) in the limit of a long pulse, i.e., the pulse having its width τ much greater than the optical period $T=2\pi/\omega$. In such a limit, $S(t)=i\Omega\int_{t_0}^{t}dt'f(t')\cos\omega t'$ can be well approximated by the first term which occurs when performing integration by parts, namely, $S(t)\simeq i(\Omega/\omega)f(t)\sin\omega t$. This can be verified most easily for, e.g., a sine-squared pulse $f(t)=\sin^2(\pi t/\tau)$ with $0\leq t\leq\tau$. A few picosecond pulse of optical frequency, which we are interested in, fulfills excellently this long-pulse approximation. Under the long-pulse approximation, we apply the Fourier-Bessel expansion to Eq. (7) and rewrite it as

$$C_j(t)=e^{i\omega_i t_0}\sum_{N=-\infty}^{+\infty}\sum_{k=1}^{n}P_{jk}P_{ik}J_N\left(\lambda_k\frac{\Omega}{\omega}f(t)\right)e^{-iN\omega t}, \quad (8)$$

where $J_N(z)$ is the Bessel function of the first kind of order N. To have a measure of population that migrates during the pulse from the initial state i, to some other state j, we calculate the time average of the population probability over an infinite time interval,

$$\begin{aligned}P_j=\langle|C_j(t)|^2\rangle_t&=\sum_{k,k'=1}^{n}P_{jk}P_{ik}P_{jk'}P_{ik'}\\&\times\sum_{N=-\infty}^{+\infty}\left\langle J_N\left((\lambda_k-\lambda_{k'})\frac{\Omega}{\omega}f(t)\right)e^{iN\omega t}\right\rangle_t\\&=\sum_{k,k'=1}^{n}P_{jk}P_{ik}P_{jk'}P_{ik'}\left\langle J_0\left((\lambda_k-\lambda_{k'})\frac{\Omega}{\omega}f(t)\right)\right\rangle_t.\end{aligned} \quad (9)$$

In the weak-field limit, defined by $\Omega/\omega\to 0$, both the Bessel function and its time average amount to 1. Then, due to the orthogonality of $P(\Sigma_k P_{jk}P_{ik}=\delta_{ji})$, the right-hand side of Eq. (9) becomes equal to the Kronecker symbol, δ_{ji}, meaning that no population leaves the initial state. Some migration of the population out of the initial l state is thus expected in the opposite limit of strong fields when $\Omega/\omega\gtrsim 1$, in conformity with the prediction of Corless and Stroud [1]. This conclusion will receive pictorial presentation later for pulses of different envelopes $f(t)$.

In the next step, we substitute the long-pulse Eq. (8) for the Rydberg-state population amplitudes into Eq. (1) for the continuum-state population amplitude. By the use of the summation relation [17]

$$J_{N-1}(z)+J_{N+1}(z)=\frac{2N}{z}J_N(z) \quad (10)$$

the latter amplitude is found as

$$C_E(t)=\frac{i}{\hbar}e^{i\omega_i t_0}\frac{\omega}{\Omega}\sum_{N=-\infty}^{+\infty}\sum_{j=1}^{n}\sum_{k=1}^{n}(N/\lambda_k)V_{Ej}P_{jk}P_{ik}\times\int_{t_0}^{t}J_N(\lambda_k\frac{\Omega}{\omega}f(t'))e^{i(E-E_n-N\hbar\omega)t'/\hbar}dt'. \quad (11)$$

As a fully analytically solvable case, we then consider the square pulse, meaning $f(t)=1$ and $t_0=0$. In this case, the resulting time integral, $\int_0^t \exp(i\alpha t')dt'$, is elementary. When taking squared modulus and then integrating over the photoelectron energy, this time integral results in $\pi\hbar t\delta_{NN'}$, in the long-pulse limit ($\omega t\gg 1$). The summation over N in the ionization probability is then performed analytically combining Eq. (10) with the relation [17]

$$\sum_{N=-\infty}^{+\infty}J_{\nu\pm N}(z)J_N(z')=J_\nu(z\mp z'). \quad (12)$$

As a result, one obtains the following differential rate for the photoelectron to be emitted into the $d\Omega$ solid angle:

$$\frac{1}{t}\frac{dW}{d\Omega}=\frac{\pi}{\hbar}d\sum_{k,k'=1}^{n}\sum_{j,j'=1}^{n}R_{k,k'}(\Omega/\omega)\times V_{Ej}P_{jk}P_{ik}(V_{Ej'}P_{j'k'}P_{ik'})^*, \quad (13)$$

where d is the density of the continuum states around the energy $E=E_n+\hbar\omega$, and

$$R_{k,k'}(\Omega/\omega)=\frac{J_1\left((\lambda_k-\lambda_{k'})\frac{\Omega}{\omega}\right)}{(\lambda_k-\lambda_{k'})\frac{\Omega}{\omega}}. \quad (14)$$

$R_{k,k'}$ is an intensity-dependent parameter, which tends to 1/2 in the weak-field limit of $\Omega/\omega\to 0$. Only in this limit, Eq. (13) converts into the standard Fermi golden rule differential rate for photoionization.

Finally, we apply the partial-wave expansion [9] for the function Ψ_E of the photoelectron emitted from the jth Rydberg state under the action of light linearly polarized in the z direction:

$$\Psi_E=\sum_{q=1_j\pm 1}\beta_q R_{Eq}(r)Y_{qm_i}(\vartheta,\varphi)Y^*_{qm_i}(\theta,\phi), \quad (15)$$

where ϑ, φ are the spherical angles of the electron radius, θ and φ the spherical angles describing the photoemission direction, and $\beta_q=i^q[\Gamma(q+1+i/y)/\Gamma(q+1-i/y)]^{1/2}$ with $y=\sqrt{2E}$ and E being the photoelectron energy in a.u. This expansion leads to

$$\sum_{j=1}^{n}V_{Ej}P_{jk}P_{ik}=\sum_{q=0}^{n}T^i_{qk}Y_{qm_i}(\theta,\phi), \quad (16)$$

where

$$T^i_{qk}=\beta^*_q P_{ik}[(1-\delta_{q,0})(e\varepsilon_0 z)^{E,q,m_i}_{n,q-1,m_i}P_{qk}+(1-\delta_{q,n-1})(1-\delta_{q,n})(e\varepsilon_0 z)^{E,q,m_i}_{n,q+1,m_i}P_{q+2,k}], \quad (17)$$

with $z^{E,l,m}_{n,l',m}$ being the standard matrix element of the z component of the electron radius between the states shown. As a result, the following final form of the differential photoionization rate is obtained:

$$\frac{1}{t}\frac{dW}{d\Omega}=\frac{\pi}{\hbar}d\sum_{q,q'=0}^{n}Z^i_{qq'}Y_{qm_i}(\theta,\phi)Y^*_{q'm_i}(\theta,\phi), \quad (18)$$

where

$$Z^i_{qq'}=\sum_{k,k'=l}^{n}R_{k,k'}(\Omega/\omega)T^i_{qk}T^{i*}_{q'k'}. \quad (19)$$

Obviously, this differential rate depends on one angle only, θ, the angle of the photoelectron emission measured with respect to the direction of linear polarization (z) of the optical pulse. As follows from the symmetry with respect to the (x,y) plane ($\theta\to\pi-\theta$), $Z^i_{qq'}$ must vanish if q and q' are numbers of different parity. We verified this requirement numerically for different Ω/ω ratios. By integrating over all photoemission directions, Eq. (18) transforms into the following total photoionization rate:

$$\frac{W}{t}=\frac{\pi}{\hbar}d\sum_{q=0}^{n}Z^i_{qq}. \quad (20)$$

Equation (18) for the differential phtoionization rate, Eq. (20) for the total ionization rate, and the previous Eq. (9) for the time-averaged Rydberg-state population are the basic equations for the study of both the $|\Delta l|=1$ migration of the population along the chain of l states and the effect of this migration on the photoionization characteristics in the model with one n manifold only.

B. Application and results

For the application, let us assume that initially ($t=t_0$) the first state of the Rydberg chain is populated only ($i=1$, $l_1=m_1=0$). Then, Eqs. (18) and (20) reduce to

$$\frac{1}{t}\frac{dW}{d\Omega}=2\gamma^{Ep}_{ns}\sum_{q,q'=0}^{n}Z_{qq'}Y_{q0}(\theta)Y^*_{q'0}(\theta) \quad (21)$$

and

$$\frac{W}{t}=2\gamma^{Ep}_{ns}\sum_{q=0}^{n}Z_{qq}, \quad (22)$$

respectively, where γ^{Ep}_{ns} is the Fermi golden rule total rate of ionization from the initial ns Rydberg state to the p continuum, whereas $Z_{qq'}$ is obtained from $Z^1_{qq'}$ by formally re-

placing $T^1_{qk} \to T_{qk} = T^1_{qk}/(e\epsilon_0 z)^{E,1,0}_{n,0,0}$. In the standard model, only the first state in the Rydberg chain is left. Then $Z_{qq'} = Z_{11} = 1/2$ and in this standard case the photoelectron angular distribution [Eq. (21)] is reduced to the familiar $|Y_{10}(\theta)|^2 \sim \cos^2\theta$ law, according to which no photoelectron is ejected in the direction perpendicular to the polarization direction of the optical pulse. Thus, the breakdown of the prohibited emission in the $\theta = \pi/2$ direction would be a spectacular photoionization proof for the population from the initial *ns* state to migrate transiently to higher-*l* Rydberg states ($l = 1,2,\ldots$) of the same *n* due to the $|\Delta l| = 1$ nonresonant transitions. As a measure of this breakdown, we introduce the intensity-dependent ratio of two photoemissions, one perpendicular and the other parallel to the direction of the laser-pulse polarization. Equation (21) gives for this ratio the expression:

$$r = \left(\frac{dW}{d\Omega}\right)_{\perp} \Big/ \left(\frac{dW}{d\Omega}\right)_{\parallel} = \frac{\sum_{q,q'=\text{even}}^{n} (-1)^{(q+q')/2} \sqrt{(2q+1)(2q'+1)} \dfrac{(q-1)!!}{q!!} \dfrac{(q'-1)!!}{(q')!!} Z_{qq'}}{\sum_{q,q'=0}^{n} \sqrt{(2q+1)(2q'+1)} Z_{qq'}}. \tag{23}$$

What one can expect is $r > 0$ when $\Omega/\omega \gtrsim 1$. Moreover, in the standard model of one-Rydberg state, the total ionization rate [Eq. (22)] converts into the common Fermi golden rule rate. Thus, a different photoionization measure for the $|\Delta l| = 1$ migration and breakdown of the standard model is the ratio

$$\rho = \frac{W}{W^S} = 2\sum_{q=0}^{n} Z_{qq}, \tag{24}$$

where $W^S = \gamma^{Ep}_{ns} t$ is the total ionization yield in the standard model. Because the Bessel function $J_1(z)$, entering Z_{qq} through $R_{k,k'}(\Omega/\omega)$, tends to zero at large arguments, we expect the ratio ρ will drop below 1 when $\Omega/\omega > 1$, pointing to a strong-field suppression of ionization due to nonresonant $|\Delta l| = 1$ migration to higher-*l* Rydberg states. As to the *W* alone, it increases slowly with the increase in laser intensity *I*, namely, as $I^{1/4} \sim (\Omega/\omega)^{1/2}$. The highest intensity in our model is, however, limited by the condition $W \ll 1$ rooted in the perturbative treatment of the bound-free transitions.

Equations (23) and (24) for *r* and ρ, respectively, are the photoionization indicators of the strong-field breakdown of the standard model with only one Rydberg state retained, namely, the initially populated *ns* state. An additional nonphotoionization indicator is, obviously, Eq. (9) for the time-averaged population, p_j, of different *l* states of the same *n*, in which $i = 1$ must be substituted now. To have *r*, ρ, and p_j in their explicit forms we need to know the eigenvalues λ_k and the components $P_{jk} = P_j(\lambda_k)$ of the corresponding eigenvectors of the *A* matrix from Eq. (4). In one case, at least, both λ_k and P_{jk} have simple analytical forms. This is the case of equal-Rabi frequencies between consecutive pairs of Rydberg states in the chain. As results from the estimation of the Rabi frequencies in Sec. I, such an approximation of equal-Rabi frequencies should work well when $n \gg 1$ and, at the same time, $l \ll n$. We take $n = 30$ to obtain illustrative model results. Thus, for the approximation in question to be reliable we should restrict the intensity parameter Ω/ω to such values at which the population from the initial 30*s* state migrates to, at most, a few nearest higher-*l* states. In some cases, these model results will be compared with exact results, i.e., those obtained without the equal-Rabi approximation. In the latter case, both λ_k and P_{jk} need to be found by standard numerical procedures. In the analytical equal-Rabi case, the *A* matrix from Eq. (4) has unit elements on the diagonals above and below the main diagonal. Following the paper by Białynicka-Birula, Białynicki-Birula, Eberly, and Shore [18], the eigenvalues of such an *A* [$\det(A - \lambda I) = D_n(\lambda) = 0$, where *I* is the unit matrix] can be found by the Laplace expanding of $D_n(\lambda)$ with respect to the last column. This expansion creates the recurrence relation $D_n(\lambda) = -\lambda D_{n-1}(\lambda) - D_{n-2}(\lambda)$, with the conditions $D_0(\lambda) = 1$ and $D_{-1}(\lambda) = D_{-2}(\lambda) = 0$. The recurrence relation mentioned defines the Chebyshev polynomial of the second kind: $D_n(\lambda) = U_n(-\lambda/2) = (-1)^n U_n(\lambda/2)$ [17]. It is then found from zeros of $U_n(\lambda/2)$ that

$$\lambda_k = -2\cos\left(\frac{k\pi}{n+1}\right), \tag{25}$$

$$P_{jk} = (-1)^{n+j+k+l}\sqrt{\frac{2}{n+1}}\sin\left(\frac{jk\pi}{n+1}\right). \tag{26}$$

For the equal-Rabi case, i.e., with Eqs. (25) and (26) used, we show in Fig. 2 the time-averaged populations p_j of different *l* states ($l = j - 1$) versus the intensity parameter Ω/ω. A variety of pulse envelopes is assumed (square $\to f(t) = 1$; $\sin^2 \to f(t) = \sin^2(\pi t/\tau_1)$; Gaussian $\to f(t) = \exp[-(t/\tau_2)^2]$; sech $\to f(t) = \text{sech}(t/\tau_3) = 2/[\exp(t/\tau_3) + \exp(-t/\tau_3)]$), all pulses of the same full width at half maximum (FWHM) $\tau_{1/2} = \tau_1/2 = 1.665\tau_2 = 2.634\tau_3 = 8$ ps nearly equal twice the Kepler period of the initially populated 30*s* state. To avoid a resonance with any lower lying hydrogenic state we took the frequency $\omega = 0.2$ a.u. (in this case, a virtual state lying in between the $n = 1$ and $n = 2$ states is reached from the initial state). The corresponding optical period *T* is such that $\tau_{1/2}/T \cong 10^4$ en-

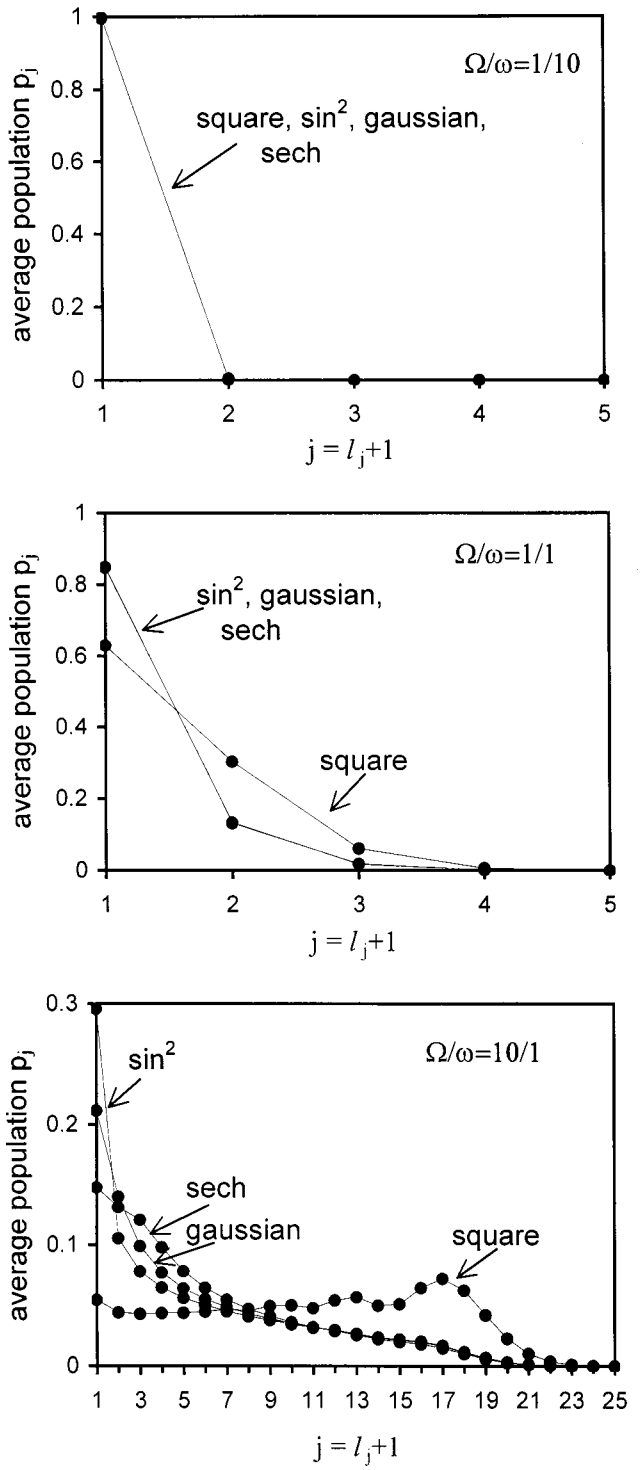

FIG. 2. The time-averaged populations p_j of different l_j states, calculated from Eq. (9), versus the pulse-strength parameter Ω/ω. The conditions: equal Rydberg-to-Rydberg couplings [Eqs. (25) and (26)], the 30s initial state, the frequency $\omega=0.2$ a.u., and the pulse duration (FWHM) of 10^4 optical periods irrespective of the pulse envelope. The results of this and other figures were obtained applying the one *n*-manifold approximation.

suring the long-pulse approximation. In Fig. 2, only the dots have physical meaning but these dots were joined by a line to guide the eye. This figure confirms the Corless and Stroud [1] predictions from their excitation model that in the strong-field region of $\Omega/\omega>1$ ($I>0.25\times10^{10}$ W/cm^2), higher-*l* states ($l\geqslant1$) of both opposite and the same parity as that of the initial Rydberg state will be populated transiently due to a sequence of nonresonant $|\Delta l|=1$ transitions. Also, Fig. 2 shows that a strong square pulse produces the *l*-state population generally different from the population produced by smooth pulses. Some differences observed in the low-*l* population for different strong smooth pulses are likely due to different area *P* under the pulse envelopes of the same FWHM [$P(\sin^2)$:P(Gaussian):P(sech)=1:1.06:2.38].

In Fig. 2, a number of different *l* states is seen to be populated for the highest Ω/ω ratio ($\Omega/\omega=10$, $I=2.5\times10^{11}$ W/cm^2). Thus, the condition $l\ll n=30$ of the validity of the approximation of equal-Rabi frequencies is expected to be violated in this case. For $\Omega/\omega=10$, we compare in Fig. 3 the time-averaged *l*-state population p_j obtained with (solid line) and without (dashed line) the equal-Rabi approximation, assuming square pulse in one case (a) and smooth sech pulse in the other case (b). As expected, some quantitative differences do occur between the approximate (solid line) and exact (dashed line) curves if *l* is high, but the general tendency remains the same. We confirmed that these differences tend to disappear quickly with decreasing the intensity parameter Ω/ω and become practically negligible at $\Omega/\omega<3$.

Through the *r* and ρ indicators [Eqs. (23) and (24)], we have an insight into the effect of the $|\Delta l|=1$ Rydberg-to-Rydberg migration on photoionization. In Fig. 4(a), we present *r* versus the intensity parameter Ω/ω, calculated with (solid line) and without (dashed line) the equal-Rabi approximation. The increase in *r* with increasing the Ω/ω parameter points to the breakdown of the $\cos^2\theta$ law of the standard model for the photoelectron distribution. At the strongest field considered ($\Omega/\omega=10$), the photoelectrons emitted in the direction perpendicular to that of the light polarization (i.e., the direction forbidden by the standard model) amount to nearly one tenth of the photoelectrons emitted in the preferred direction of the light polarization. Figure 4(b) shows the bulge of the photoelectron angular distribution in the perpendicular direction when coming from the weak field ($\Omega/\omega=1/10$) to the strong field ($\Omega/\omega=10/1$). The light-polarization direction, with respect to which the photoemission angle θ is measured, is marked by the vertical arrow. As in Fig. 4(a), the solid (dashed) line corresponds to the calculations performed with (without) the equal-Rabi approximation.

In Fig. 5(a), we present the other photoionization indicator of the $|\Delta l|=1$ Rydberg-to Rydberg couplings, namely ρ in its dependence on the intensity parameter Ω/ω. The same is shown in Fig. 5(b) but with a different horizontal scale. Again, the solid (dashed) line corresponds to the results obtained with (without) the equal-Rabi approximation. The suppression of the total photoionization due to the $|\Delta l|=1$ Rydberg-to-Rydberg couplings starts evidently when the intensity parameter Ω/ω approaches 1. At $\Omega/\omega=10$, the suppression is by as much as the factor of 5.85. In Fig. 5(c) this suppression is shown along a different line, i.e., we compare the total ionization rate W/t obtained from Eq. (22) (i.e., with the inclusion of the $|\Delta l|=1$ Rydberg-to-Rydberg cou-

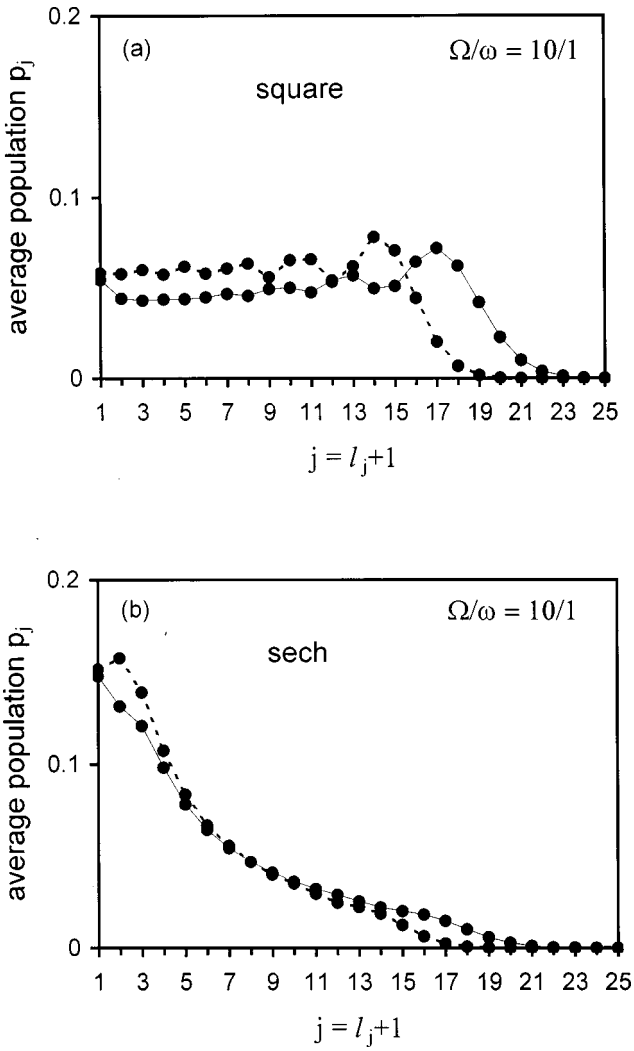

FIG. 3. The strong-field ($\Omega/\omega=10$) time-averaged populations p_j of different l_j states, calculated with (solid line) and without (dashed line) the approximation of equal Rydberg-to-Rydberg couplings, for square pulse (a) and sech pulse (b).

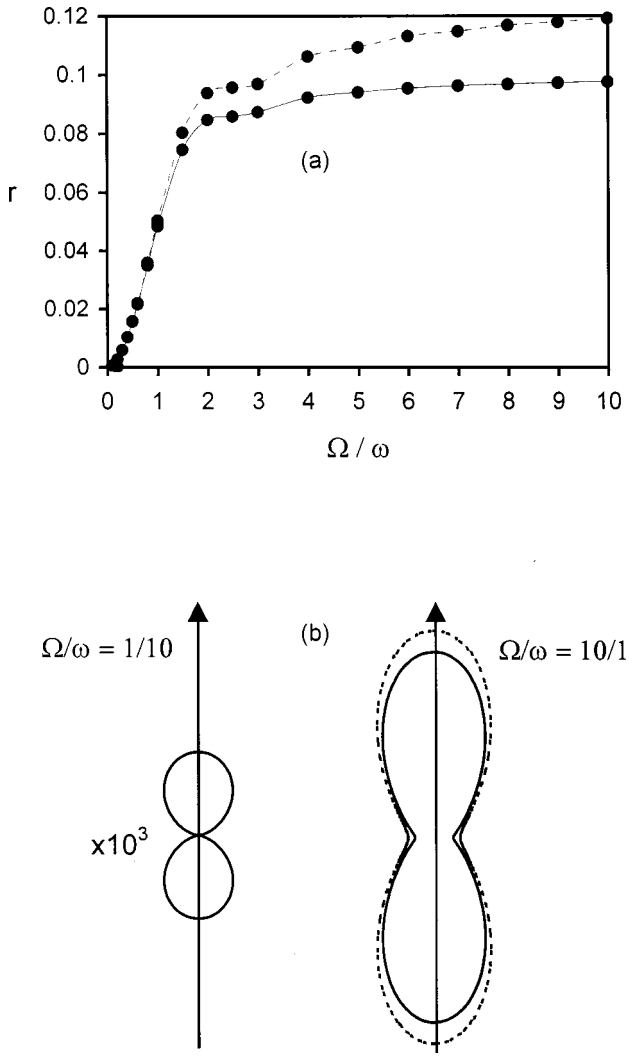

FIG. 4. The ratio r [Eq. (23)] of the photoemissions in two orthogonal directions, one perpendicular and the other along the light polarization direction, versus the pulse-strength parameter Ω/ω (a); the weak-field ($\Omega/\omega=0.1$) and the strong-field ($\Omega/\omega=10$) photoelectron angular distributions pointing to the bulge of the photoemission in the $\theta=\pi/2$ direction (b). The solid (dashed) line corresponds to the calculations with (without) the approximation of equal Rydberg-to-Rydberg couplings. The case is of the long square pulse of $\omega=0.2$ a.u.

plings) with the rate $W^S/t=\gamma_{30s}^{Ep}$ of the standard model. Let us notice that now there is $(\Omega/\omega)^2$ instead of Ω/ω on the horizontal axis. Figure 5(c) shows clearly the departure from the standard linear dependence of the photoionization rate on laser intensity. As follows from Fig. 5(c), a picosecond pulse of the maximum intensity considered $[(\Omega/\omega)^2=100\rightarrow I=2.5\times10^{11}\,\mathrm{W/cm^2}]$ gives the ionization probability $W\ll1$, as required by our perturbative treatment of the bound-free transitions.

In Fig. 6, we give an explanation of the results of Figs. 4 and 5 in terms of the dependence of the $Z_{qq'}$ parameters [Eq. (19) and the note after Eq. (22)] on the field strength. We concentrate on the diagonal parameters Z_{qq} only, which are the weights at which the squared spherical harmonics, $|Y_{qo}|^2$, enter the photoelectron angular distribution [Eq. (21)]. According to Eq. (22), these diagonal parameters are the only ones determining the total ionization rate. Figure 6 shows that, in weak fields, only $Z_{11}=1/2$ is essential and determines completely the standard $|Y_{10}(\theta)|^2\sim\cos^2\theta$ photoelectron distribution and the standard Fermi golden rule total ionization rate. However, with increasing field strength, Z_{11} begins to decrease monotonically and the relative contributions of $Z_{22}(Y_{20})$, $Z_{00}(Y_{0,0})$, and $Z_{33}(Y_{30})$ become nonnegligible. The Z_{22}, Z_{00}, and Z_{33} contributions are what predominantly modify, in strong fields, the results of the standard model of photoionization with no Rydberg-to-Rydberg couplings. The effect of Z_{qq} with higher q is minor due to a rapid decrease of the bound-free matrix element $z_{n,l\pm1,0}^{E,l,0}$ with increasing angular momentum quantum number l.

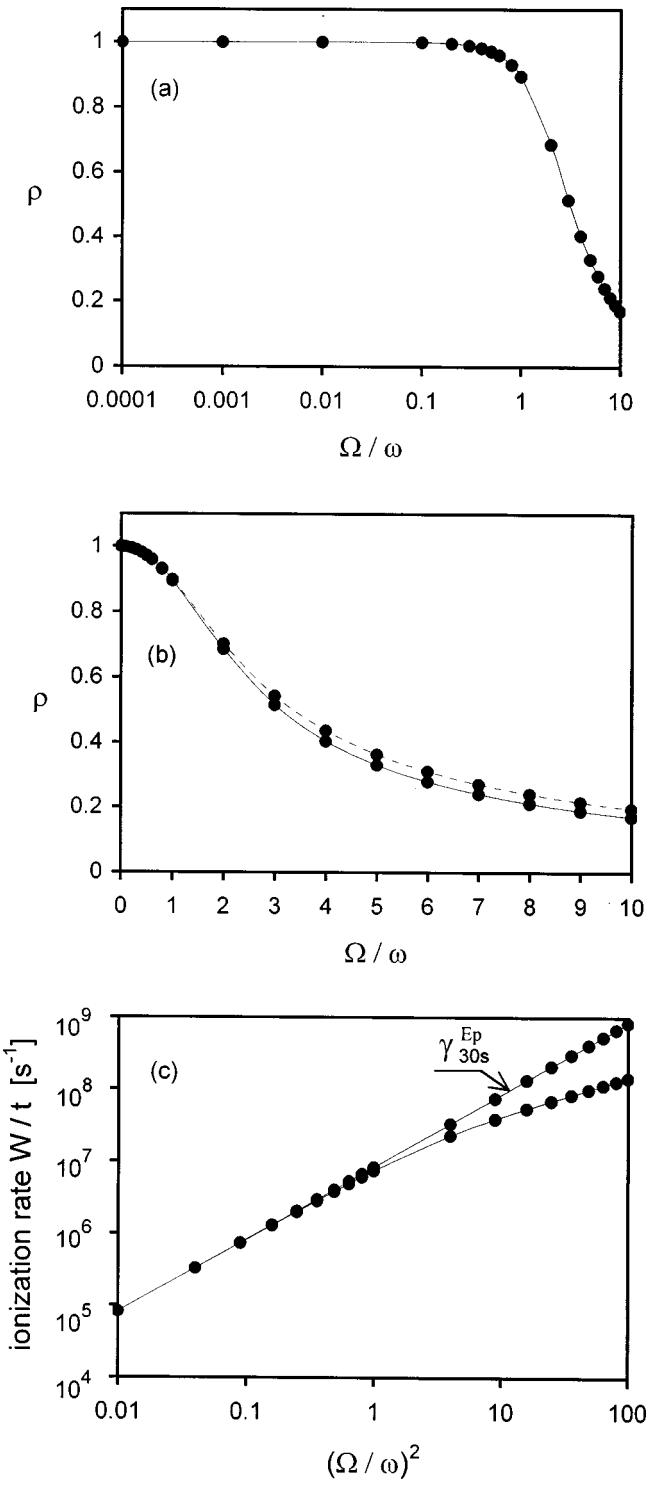

FIG. 5. The ratio ρ [Eq. (24)] of two total ionization rates, one calculated with the inclusion of the $|\Delta l|=1$ Rydberg-to-Rydberg couplings (the present model) and the other calculated without these couplings (the standard model), versus the pulse-strength parameter Ω/ω (a), (b); the present ionization rate W/t [Eq. (22)] and the standard ionization rate γ^{Ep}_{30s} versus the $(\Omega/\omega)^2$ parameter proportional to laser intensity (c). Solid (dashed) line corresponds to the calculations with (without) the approximation of equal Rydberg-to-Rydberg couplings. The case is of the long square pulse of $\omega = 0.2$ a.u.

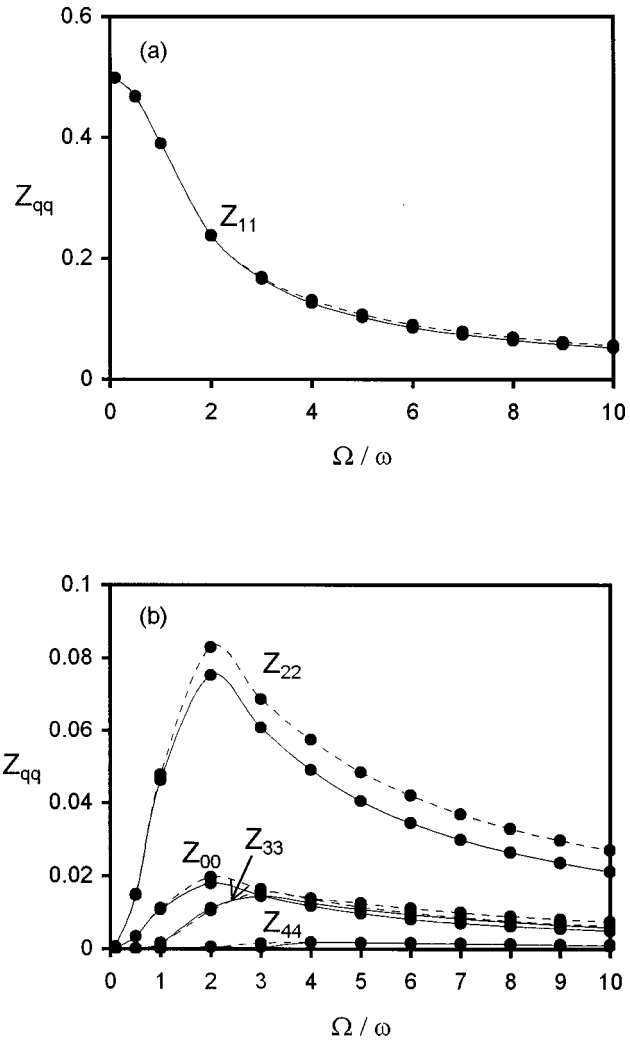

FIG. 6. The diagonal parameters Z_{qq} [Eq. (19) and the note after Eq. (22)] versus the field-strength parameter Ω/ω. The case is of the long square pulse of $\omega = 0.2$ a.u. Solid (dashed) line corresponds to the calculations with (without) the approximation of equal Rydberg-to-Rydberg couplings.

III. EFFECT OF ADDITIONAL *n* MANIFOLDS AND CONCLUSION

The photoionization results presented and discussed above, particularly those concerning the electron ejection in the ''forbidden'' directions and the ionization suppression, look very exciting. However, we cannot forget that they were obtained within the simplified model which included only one n manifold. Fortunately, there is one case, at least, in which the general model from Fig. 1, with a number of additional n manifolds neighboring to the initially occupied n_0 manifold, can also be solved analytically but in an approximate, rather than exact, way. The case concerns the pulses shorter than the Kepler period of the initially prepared Rydberg state (n_0), but still much longer than the optical period for the long-pulse approximation to be valid. In this case the neighboring n manifolds are not resolved by the pulse and can be considered as degenerate with the n_0 manifold. Under this condition, Eq. (3), with the bound-free term dropped,

remains valid for the neighboring n manifolds as well, provided that we replace $C_j \rightarrow C_{nj}$, $C_{j'} \rightarrow C_{n'j'}$, $\Omega_{jj'} \rightarrow \Omega_{nj,n'j'}$ and sum not only over j' but also over n'. Then, by the use of the quasiclassical dipole matrix elements between high Rydberg states [1,19], one finds the approximate relation $\Omega_{nj,n'j'} = f(\Delta n)\Omega_{jj'}$, valid for $\Delta n = n' - n \neq 0$, where $f(\Delta n) = (2/3\Delta n)J'_{\Delta n}(\Delta n)$, and $J'_{\Delta n}(\Delta n)$ stands for the derivative of the Bessel function. For its validity, this relation needs $\Delta n \ll n_0$ and $j = l + 1 \ll n_0$. Applying this relation, we sum the modified Eq. (3) over n in the next step. Such a procedure results in an equation for $B_j = \Sigma_n C_{nj}$ which has exactly the same structure as the original Eq. (3) with the replacement $\Omega_{jj'} \rightarrow \xi\Omega_{jj'}$, where $\xi = 1 - \Sigma_{\Delta n} f(\Delta n)$. As a result, the solution for B_j is found to take the form of Eq. (7). Moreover, due to a weak n dependence of bound-free matrix elements from high Rydberg states [19], one sees that the right-hand side of the modified Eq. (1) for the photoionization amplitude is expressed by B_j. All this means that the solutions for the photoionization characteristics, found in Sec. II by applying the one n-manifold approximation, remain unchanged when including the neighboring n manifolds and assuming the pulse shorter than the initial-state Kepler period. The only thing we have to do is to rescale $\Omega \rightarrow \xi\Omega$ in Eq. (14) and Figs. 4–6. Since $\xi < 1$ and can be damped to a very small value when including a lot of different n manifolds, the conclusion is that, at a given intensity, the neighboring n manifolds diminish drastically the photoionization effects obtained within the simpler model with one n manifold only. Due to our highly approximate approach, when obtaining the damping parameter ξ, we are not able to answer the question whether complete cancellation of these effects is possible. To answer this question, either numerical solution to the model of Fig. 1 or the experimental verification of the exact results of the one n manifold photoionization model is required. Along these lines, the applicability of the one n-manifold approximation of Corless and Stroud [1] to the problems of high-n Rydberg-state photoionization is expected to be established.

ACKNOWLEDGMENT

Financial support from the Polish Committee for Scientific Research under Grant No. 2 PO3B 078 12 is acknowledged.

[1] J. D. Corless and C. R. Stroud, Jr., Phys. Rev. Lett. **79**, 637 (1997).
[2] H. A. Bethe and E. E. Salpeter, *Quantum Mechanics of One- and Two-Electron Atoms* (Springer Verlag, Berlin, 1957), Chap. IV.
[3] R. Grobe, G. Leuchs, and K. Rzażewski, Phys. Rev. A **34**, 1188 (1986).
[4] G. K. Ivanov, G. V. Golubkov, and D. M. Manakov, Zh. Eksp. Teor. Fiz. **106**, 1306 (1994) [JETP **79**, 707 (1994)].
[5] K. Im, R. Grobe, and J. H. Eberly, Phys. Rev. A **49**, 2853 (1994).
[6] M. V. Fedorov, M. M. Tehranchi, and S. M. Fedorov, J. Phys. B **29**, 2907 (1996).
[7] R. Parzyński and A. Wójcik, Laser Phys. **7**, 551 (1997).
[8] A. Wójcik, R. Parzyński, and A. Grudka, Phys. Rev. A **55**, 2144 (1997).
[9] R. Parzyński and A. Grudka, Phys. Rev. A **58**, 1335 (1998); **59**, 893 (1999).
[10] R. Parzyński and S. Wieczorek, Phys. Rev. A **58**, 3051 (1998).
[11] M. O. Scully and M. S. Zubairy, *Quantum Optics* (Cambridge University Press, Cambridge, England, 1997), Chap. 5.
[12] W. Becker, Opt. Commun. **56**, 107 (1985).
[13] C. Leubner and P. Zoller, J. Phys. B **13**, 3613 (1980).
[14] W. E. Lamb, Jr., R. R. Schlicher, and M. O. Scully, Phys. Rev. A **36**, 2763 (1987).
[15] C. Cohen-Tannoudji, J. Dupont-Roc, and G. Grinberg, *Photons and Atoms: Introduction to Quantum Electrodynamics* (Wiley, New York, 1987), Chap. IV.
[16] D. G. Zill *Differential Equations with Boundary-Value Problems* (Prindle, Weber and Schmidt, Boston, 1986), Chap. 8.
[17] I. M. Ryzhik and I. S. Gradshteyn, *Tablicy Integralov, Sum, Ryadov i Proizvedeniy* (Nauka, Moskwa, 1971), pp. 984, 994, 1046.
[18] Z. Białynicka-Birula, I. Białynicki-Birula, J. H. Eberly, and B. W. Shore, Phys. Rev. A **16**, 2048 (1977).
[19] N. B. Delone, S. P. Goreslavsky, and V. P. Krainov, J. Phys. B **27**, 4403 (1994).